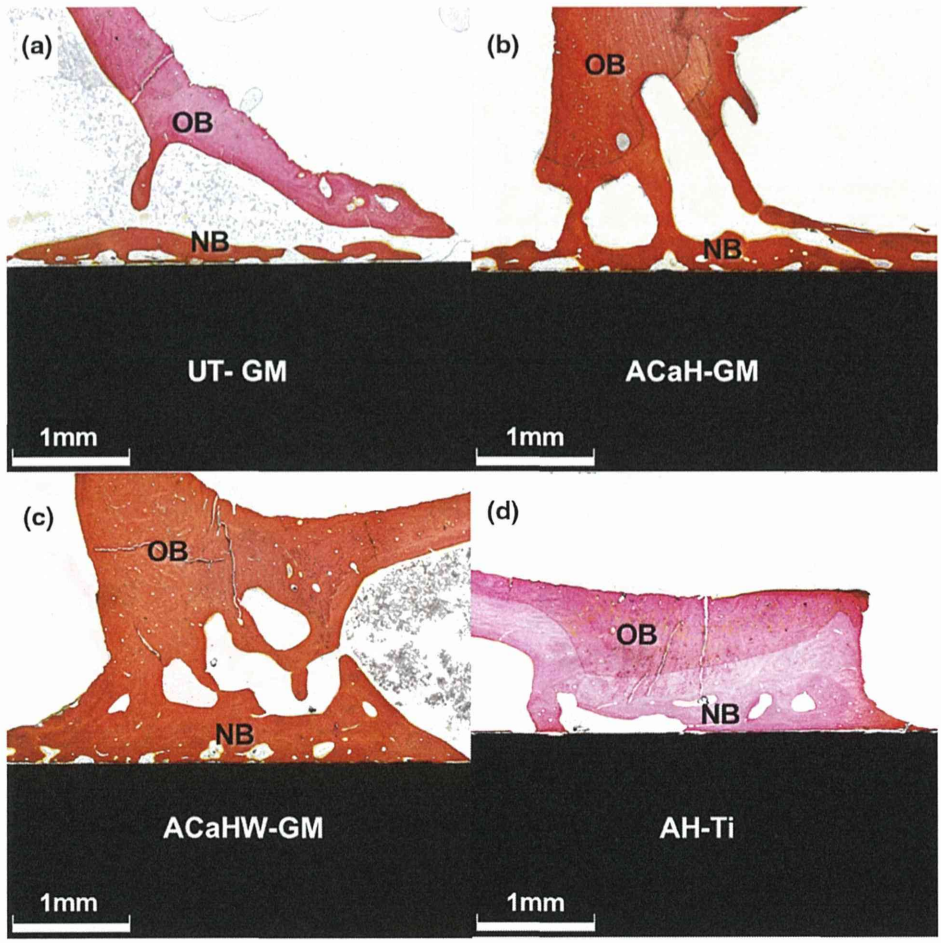

Fig. 6 Surface staining of the bone–implant interface with Stevenel's blue and Van Gieson's picrofuchsin at 26 weeks. (**a**) UT-GM, (**b**) ACaH-GM, (**c**) ACaHW-GM, and (**d**) AH-Ti. *OB* original bone; *NB* new bone

ACaH-GM samples, a layer of fibrous tissue existed at the bone–implant interface 8 weeks after surgery, and the bone tissue made only partial contact with the implant at 16 and 26 weeks. These results confirm that ACaHW treatment of gum metal enhanced its bone-bonding ability.

Both ACaHW-GM and ACaH-GM have nanometer-scale fine network structures on their surfaces (Fig. 2b, c). However, the failure load of ACaHW-GM was higher than that of ACaH-GM at all time periods. This means the bioactivity of gum metals cannot be attributed to their surface structures. In previous studies, the surfaces of ACaHW-GM showed apatite-forming abilities when soaked in SBF for 3 days; this behavior was not seen for the ACaH-GM plates [11]. It has been shown that Ti and Ti-based alloys with surfaces conducive to apatite formation in SBF bond to living bone through the apatite layer that forms on their surfaces in the living body [12–14]. These findings suggest that it is the apatite-forming ability of the ACaHW-GM samples that enables them to tightly bond to living bone in the body.

We suggest that apatite forms on the surfaces of ACaHW-GM samples but not on ACaH-GM samples, because of differences in chemistry. When the gum metal is subjected to $CaCl_2$ treatment after NaOH treatment, the calcium ions can substitute for sodium in the sodium hydrogen titanate formed by the NaOH treatment; the result of this is a layered calcium hydrogen titanate structure, $Ca_xH_{2-2x}Ti_3O_7$, on the surface. This calcium hydrogen titanate is then transformed into various forms of calcium titanate (such as $CaTi_4O_9$, $CaTi_2O_4$, and $CaTi_2O_5$), calcium niobate (such as $Ca_2Nb_2O_7$ and $CaNb_2O_6$), rutile, and anatase by the subsequent heat treatment. The gum metal treated to this point did not show apatite-forming ability in SBF, probably because of the extremely slow diffusion of calcium ions from the calcium titanates and niobates, as has been previously seen for the calcium titanate formed on the surface of Ti–15Zr–4Nb–4Ta

alloy [20]. The final water treatment step results in some of the calcium ions in the surface layer being exchanged for oxonium ions, without an apparent change in the crystal phases. Thus, the resultant phases can be described as $Ca_xH_{2-2x}Ti_4O_9$, $Ca_xH_{2-2x}Ti_2O_4$, and $Ca_xH_{2-2x}Ti_2O_5$ for the calcium-deficient calcium titanate, and $Ca_xH_{4-2x}Nb_2O_7$ and $Ca_xH_{2-2x}Nb_2O_6$ for the calcium-deficient calcium niobate. The gum metal treated in this way (the ACaHW-GM samples) exhibited a high capacity for apatite formation in SBF probably because of the increased mobility of the calcium ions in the calcium titanates and niobates caused by incorporation of the oxonium ions [11].

In our animal study, the ACaHW-GM samples showed good affinity for bone tissue, and histological examinations demonstrated biocompatibility. The ACaHW-GM plate, which is V-free Ti alloy, seems to be nontoxic with good osteoconductivity.

To resolve stress shielding after cementless total hip arthroplasties, which can arise because of differences in Young's modulus between the stem and human cortical bone, the Young's modulus of the alloy used for the stem alloy needs to be close to the Young's modulus of human cortical bone [7–9]. To precisely assess local stress–strain distributions in geometrically complex structures, finite element methods are a standard tool used in biomedical engineering [21]. A finite element model (FEM) of a biomimetic stem (composed of hydroxyapatite–coated carbon fibers), with material properties similar to those of a cortical bone (Young's modulus is 5–30 GPa) was constructed [22]. Three static load cases representing slow walking, stair climbing, and gait in a healthy individual were considered. Stress shielding was evaluated and compared with the results of a similar FEM for a titanium alloy (Ti–6Al–4V). The composite stems allowed for reduced stress shielding when compared with a traditional Ti–6Al–4V stem.

The Young's modulus of the gum metal used in this study is 55 GPa, much closer to that of human cortical bone (10–30 GPa) than Ti–6Al–4V alloy (110 GPa), so the gum metal should reduce stress shielding in the femur, and thus decrease thigh pain. Further animal studies and FEM analyses are needed to test this hypothesis.

Thus, ACaHW-GM should be useful for developing novel orthopedic implants such as cementless joint replacements or dental implants, because of its good bone bonding ability. The gum metal should also prevent stress shielding under loaded conditions because it has a low Young's modulus.

5 Conclusions

A gum metal with composition Ti–36Nb–2Ta–3Zr–0.3O exhibited bone bonding ability in vivo after successive NaOH, $CaCl_2$, heat (700 °C), and water treatments. The present results suggest that the gum metal may be useful in novel orthopedic implants or dental implants because of its excellent bioactivity. The low Young's modulus of gum metal mean that stress shielding under loaded conditions should be able to be prevented.

References

1. Niinomi M, Hattori T, Morikawa K, Kasuga T, Suzuki A, Fukui H, et al. Development of low rigidity β-type titanium alloy for biomedical applications. Mater Trans. 2002;43(12):2970–7.
2. Head WC, Bauk DJ, Emerson RH Jr. Titanium as the material of choice for cementless femoral components in total hip arthroplasty. Clin Orthop Relat Res. 1995;311:85–90.
3. Long M, Rack HJ. Titanium alloys in total joint replacement–a materials science perspective. Biomaterials. 1998;19(18):1621–39.
4. Mont MA, Hungerford DS. Proximally coated ingrowth prostheses. A review. Clin Orthop Relat Res. 1997;344:139–49.
5. Nourbash PS, Paprosky WG. Cementless femoral design concerns. Rationale for extensive porous coating. Clin Orthop Relat Res. 1998;355:189–99.
6. Glassman AH, Bobyn JD, Tanzer M. New femoral designs: do they influence stress shielding? Clin Orthop Relat Res. 2006;453:64–74.
7. Andrew TA, Flanagan JP, Gerundini M, Bombelli R. The isoelastic, noncemented total hip arthroplasty. Preliminary experience with 400 cases. Clin Orthop Relat Res. 1986;206:127–38.
8. Butel J, Robb JE. The isoelastic hip prosthesis followed for 5 years. Acta Orthop Scand. 1988;59(3):258–62.
9. Niinimaki T, Jalovaara P. Bone loss from the proximal femur after arthroplasty with an isoelastic femoral stem. BMD measurements in 25 patients after 9 years. Acta Orthop Scand. 1995;66(4):347–51.
10. Saito T, Furuta T, Hwang JH, Kuramoto S, Nishino K, Suzuki N, et al. Multifunctional alloys obtained via a dislocation-free plastic deformation mechanism. Science. 2003;300(5618):464–7. doi:10.1126/science.1081957.
11. Yamaguchi S, Kizuki T, Takadama H, Matsushita T, Nakamura T, Kokubo T. Formation of a bioactive calcium titanate layer on gum metal by chemical treatment. J Mater Sci - Mater Med. 2012;23(4):873–83. doi:10.1007/s10856-012-4569-7.
12. Nishiguchi S, Kato H, Fujita H, Kim HM, Miyaji F, Kokubo T, et al. Enhancement of bone-bonding strengths of titanium alloy implants by alkali and heat treatments. J Biomed Mater Res. 1999;48(5):689–96.
13. Kim HM, Miyaji F, Kokubo T, Nakamura T. Preparation of bioactive Ti and its alloys via simple chemical surface treatment. J Biomed Mater Res. 1996;32(3):409–17. doi:10.1002/(SICI)1097-4636(199611)32:3<409:AID-JBM14>3.0.CO;2-B.
14. Fukuda A, Takemoto M, Saito T, Fujibayashi S, Neo M, Yamaguchi S, et al. Bone bonding bioactivity of Ti metal and Ti-Zr-Nb-Ta alloys with Ca ions incorporated on their surfaces by simple chemical and heat treatments. Acta Biomater. 2011;7(3):1379–86. doi:10.1016/j.actbio.2010.09.026.
15. Niinomi M. Recent metallic materials for biomedical applications. Metall and Mat Trans A. 2002;33(3):477–86. doi:10.1007/s11661-002-0109-2.
16. Kim HM, Miyaji F, Kokubo T, Nakamura T. Effect of heat treatment on apatite-forming ability of Ti metal induced by alkali treatment. J Mater Sci - Mater Med. 1997;8(6):341–7.
17. Nishiguchi S, Nakamura T, Kobayashi M, Kim HM, Miyaji F, Kokubo T. The effect of heat treatment on bone-bonding ability of alkali-treated titanium. Biomaterials. 1999;20(5):491–500.

18. Fujibayashi S, Nakamura T, Nishiguchi S, Tamura J, Uchida M, Kim HM, et al. Bioactive titanium: effect of sodium removal on the bone-bonding ability of bioactive titanium prepared by alkali and heat treatment. J Biomed Mater Res. 2001;56(4):562–70.
19. Nakamura T, Yamamuro T, Higashi S, Kokubo T, Itoo S. A new glass–ceramic for bone replacement: evaluation of its bonding to bone tissue. J Biomed Mater Res. 1985;19(6):685–98. doi:10.1002/jbm.820190608.
20. Yamaguchi S, Takadama H, Matsushita T, Nakamura T, Kokubo T. Apatite-forming ability of Ti–15Zr–4Nb–4Ta alloy induced by calcium solution treatment. J Mater Sci - Mater Med. 2010;21(2):439–44. doi:10.1007/s10856-009-3904-0.
21. Sakai R, Itoman M, Mabuchi K. Assessments of different kinds of stems by experiments and FEM analysis: appropriate stress distribution on a hip prosthesis. Clin. Biomech. (Bristol, Avon). 2006;21(8):826–33. doi:10.1016/j.clinbiomech.2006.03.008.
22. Caouette C, Yahia L, Bureau MN. Reduced stress shielding with limited micromotions using a carbon fibre composite biomimetic hip stem: a finite element model. Proc Inst Mech Eng [H]. 2011;225(9):907–19. doi:10.1177/0954411911412465.

J Mater Sci: Mater Med (2014) 25:1505–1517
DOI 10.1007/s10856-014-5181-9

Development of a novel calcium phosphate cement composed mainly of calcium sodium phosphate with high osteoconductivity

Masashi Tanaka · Mitsuru Takemoto · Shunsuke Fujibayashi · Toshiyuki Kawai · Masako Tsukanaka · Kimiaki Takami · Satoshi Motojima · Hikaru Inoue · Takashi Nakamura · Shuichi Matsuda

Received: 21 November 2013 / Accepted: 14 February 2014 / Published online: 27 March 2014

Abstract Two novel calcium phosphate cements (CPC) have been developed using calcium sodium phosphate (CSP) as the main ingredient. The first of these cements, labeled CAC, contained CSP, α-tricalcium phosphate (TCP), and anhydrous citric acid, whereas the second, labeled CABC, contained CSP, α-TCP, β-TCP, and anhydrous citric acid. Biopex®-R (PENTAX, Tokyo, Japan), which is a commercially available CPC (Com-CPC), and OSferion® (Olympus Terumo Biomaterials Corp., Tokyo, Japan), which is a commercially available porous β-TCP, were used as reference controls for analysis. In vitro analysis showed that CABC set in 5.7 ± 0.3 min at 22 °C and had a compressive strength of 86.0 ± 9.7 MPa after 5 days. Furthermore, this material had a compressive strength of 26.7 ± 3.7 MPa after 2 h in physiologic saline. CAC showed a statistically significantly lower compressive strength in the presence of physiologic saline and statistically significantly longer setting times than those of CABC. CABC and CAC exhibited apatite-forming abilities in simulated body fluid that were faster than that of Com-CPC. Samples of the materials were implanted into the femoral condyles of rabbits for in vivo analysis, and subsequent histological examinations revealed that CABC exhibited superior osteoconductivity and equivalent bioresorbability compared with Com-CPC, as well as superior osteoconductivity and bioresorbability compared with CAC. CABC could therefore be used as an alternative bone substitute material.

M. Tanaka (✉) · M. Takemoto · S. Fujibayashi · T. Kawai · M. Tsukanaka · S. Matsuda
Department of Orthopaedic Surgery, Graduate School of Medicine, Kyoto University, 54 Kawahara-cho, Shougoin, Sakyou-ku, Kyoto 606-8507, Japan
e-mail: masashit@kuhp.kyoto-u.ac.jp

K. Takami · S. Motojima · H. Inoue
Olympus Terumo Biomaterials Corp., Shinjuku Monolith, 2-3-1 Nishi-Shinjuku, Shinjuku-ku, Tokyo 163-0914, Japan

T. Nakamura
National Hospital Organization Kyoto Medical Center, 1-1 Fukakusa Mukaihata-cho, Fushimi-ku, Kyoto 612-8555, Japan

1 Introduction

Autogenic bone grafts have been used in a number of areas, including bone replacement and for the enhancement of fracture repair and bone loss resulting from large defects after the fracture or the curettage of bone tumors [1]. Bone grafts of this type still represent the gold standard in terms of the treatment of bone loss because they afford good levels of osteoconductive capacity in the harvested material [2–4]. There are, however, several disadvantages associated with the use of autografts including their limited supply, the requirement for second-site surgery for autograft harvesting, donor site morbidity [4, 5], and the difficulty in obtaining the desired shape of the defective part.

Calcium phosphate cement (CPC) was developed in 1985 [6], and subsequently used in a number of different areas, including bone replacement, dentistry, craniofacial and maxillofacial applications, and vertebroplasty and kyphoplasty applications [7] where it has been used to solve the problems described above for autografts. Furthermore, this material has been reported to exhibit good biocompatibility [8, 9].

The conventional CPC of an apatite cement is widely used as a bone substitute because of its high affinity for bone tissues, its adaptation to the geometry of the defective part [10], and its high mechanical strength. However, there are several disadvantages associated with CPC, including

(1) it takes a long time to reach its maximum compressive strength, with Biopex®-R, for example, requiring 3 days, and the initial strength prior to this time may be insufficient, so additional fixation devices or prolonged bed rest may be required following an operation [10]; (2) they are difficult to handle during the setting time because they can crumble and therefore require an extended setting time, with Biopex®-R, for example, requiring a setting time of over 11 min [10]; (3) if they are contaminated with blood in vivo, they can require a much longer time to harden and the magnitude of their compressive strength can be reduced significantly [10]; (4) their osteoconductivity is not sufficient for clinical use, with non-union between CPCs and the surrounding bone tissues often observed [11], and (5) they possess very little bioresorbability in a living body because their final reaction product is mainly hydroxyapatite (HA) [7].

The first CPC containing calcium sodium phosphate (CSP) was reported in 2001 [12]. Doi et al. reported the formation of a CPC composed of CSP and tetracalcium phosphate and β-tricalcium phosphate (TCP). Solutions of CSP are alkaline because CSP contains sodium, and citric acid or malic acid can therefore be used as a hardening accelerator for CPC materials containing CSP. It is well known that the mixing of citric acid with calcium ions in an aqueous solution leads to the instantaneous formation of a chelate between the two species, with hardening then occurring rapidly [13]. When a powdered material containing CSP is mixed with an aqueous solution of malic acid or citric acid, the resulting cement sets in 3.0 or 6.25 min at room temperature. In contrast, conventional apatite CPCs only harden as a consequence of the hydrolysis of calcium phosphate, and therefore require longer hardening times. These materials are also difficult to handle during the setting process. It was therefore envisaged that CPCs containing CSP with shorter setting times would be easier to handle during the setting process. CPCs of this type could also avoid the issues associated with blood contamination that can occur during the long setting times required of conventional apatite CPCs.

In an in vitro trial reported in 2004 [14]. Four test materials were created from CSP and its derivatives, including (1) R1 composed of CSP ($CaNaPO_4$); (2) R1/M2 composed of CSP and $MgNaPO_4$; (3) R1 + SiO_2 composed of CSP and 9 % SiO_2 (wt%); and (4) R17 composed of $Ca_2KNa(PO_4)_2$. R1 and R1 + SiO_2 had the greatest effect of all of the materials tested in this particular study on osteoblastic differentiation and induced the expression of higher levels of osteogenic proteins than the other materials. To date, however, there have been no in vivo trials demonstrating the biocompatibility of CSP.

In this study, we have developed novel CPCs made predominantly of calcium sodium phosphate (CSP), α-TCP, and citric acid, both with and without β-TCP. Based on the results of previous studies, the inclusion of CSP could lead to high osteoconductivities and short hardening times with malic acid or citric acid. Malic acid is more acidic than citric acid, and its chelate reactions occur at a greater rate than those of citric acid, although the setting times can be too short to allow for effective clinical use. With this in mind, we decided to use citric acid in the current study. The chelate species formed between CSP and citric acid, in addition to tetracalcium phosphate and β-TCP, has been reported to exhibit low compressive strength (28 MPa) [12]. With this in mind, we investigated the addition of a combination of both α-TCP and β-TCP (sample: CABC) and α-TCP only (sample: CAC) to improve the mechanical properties of the CPCs.

The aim of this study was to evaluate the physical properties of these novel CPCs, in vivo osteoconductivity, and material absorptivity. Biopex®-R, which is a commercially available CPC (Com-CPC), and OSferion®, which is a commercially available porous β-TCP (P-CP), were used as the reference materials. The Biopex®-R (Com-CPC) used in the current study consisted of the following powdered components: α-TCP 74.9 wt%, tetracalcium phosphate 18 wt%, dicalcium phosphate dihydrate 5 wt%, HA 2 wt% and magnesium phosphate 0.1 wt%, as well as the following liquid components: water 82.7 wt%, disodium succinate 12 wt%, sodium chondroitin sulfate 5 wt% and sodium hydrogensulfate 0.3 wt%. When the powder was mixed with the malaxation liquid it turned into a paste, which hardened over time through hydration and changes in its structure to become more HA-like [10]. The OSferion® (P-CP) used in the current study was composed of β-TCP only and existed as a porous body with 75 % porosity.

2 Materials and methods

2.1 Materials

Two new CPCs were produced in the current study (Table 1). The first of these CPCs (CABC) consisted of the following powdered components: 41.2 wt% CSP (the manufacturing process is described in the following paragraph), 17.6 wt% α-TCP (Taihei Chemical Industrial Co., Ltd., Osaka, Japan), 17.6 wt% β-TCP (OSferion®) and 11.8 wt% anhydrous citric acid (Komatsuya Corporation, Osaka, Japan), and the following liquid components: 10.6 wt% distilled water and 1.2 wt% glycerol (Junsei Chemical Co., Ltd., Tokyo, Japan). The second CPC (CAC) consisted of the following powdered components: 50.0 wt% CSP, 21.4 wt% α-TCP, and 14.4 wt% anhydrous citric acid, as well as the following liquid components: 12.8 wt% distilled water and 1.4 wt% glycerol.

Table 1 Chemical composition of novel CPCs (CABC and CAC)

Novel CPC	Chemical composition : wt%					
	Powdered components				Liquid components	
	CSP	α-TCP	β-TCP	Anhydrous citric acid	Distilled water	Glycerol
CABC	41.2	17.6	17.6	11.8	10.6	1.2
CAC	50.0	21.4	0.0	14.4	12.8	1.4

CABC Novel CPC made of CSP, α-TCP, β-TCP, and anhydrous citric acid powdered components, *CAC* Novel CPC made of CSP, α-TCP, and anhydrous citric acid powdered components, *CSP* calcium sodium phosphate, *TCP* tricalcium phosphate

The CSP was made of 54.4 g (2.36 wt%) of dibasic calcium hydrogen phosphate dehydrate (Tomita Pharmaceutical Co., Ltd., Tokushima, Japan), 109 g (4.72 wt%) of calcium carbonate (Ube Material Industries, Ltd., Yamaguchi, Japan), 145 g (6.28 wt%) of disodium phosphate dodecahydrate (Yoneyama Chemical Industry Co., Ltd., Osaka, Japan), and 2,000 g (86.64 wt%) of distilled water (Table 2). These materials were placed in a nylon pot mill with 10 kg of zirconia balls (10 mm in diameter) and mixed at 70 rpm for 23 h. The resulting slurry was dried at 80 °C for 24 h, before being pulverized in a bowl and sieved to remove particles of less than 300 μm in diameter. The remaining particles were then burned at 1,050 °C for 10 h in a desktop muffle furnace KDF-P90 (Denken Co., Ltd., Kyoto, Japan) with heating rate 300 °C/hour before being pulverized in a bowl to give the CSP powder.

Com-CPC (Biopex®-R) and P-CP (OSferion®) were used in the current study for comparison. In total, four materials were examined in this study, including (1) CABC, (2) CAC, (3) Com-CPC, and (4) P-CP.

2.2 Material characterization

2.2.1 Scanning electron microscopy and X-ray diffraction of the CSP powder

The morphologies of the CSP powders were examined by scanning electron microscopy (SEM, S-4700; Hitachi Ltd., Tokyo, Japan), and their crystal phases were determined from their X-ray diffraction (XRD) patterns using Miniflex (Rigaku Corporation, Tokyo, Japan). The powders were pulverized with a mortar and press-fitted onto the aluminum sample holders of the XRD apparatus. The scan speed was set at 3°/minute with a scan range of 10–80°. The peaks were compared to those ICDD PDF 2-904 (CaNaPO4) and ICDD PDF 11-236 [$Ca_6Na_3(PO_4)_5$]. The phase compositions were determined using the Rietveld refinement.

2.2.2 Setting time at various room temperatures

The setting times were measured for CABC, CAC, and Com-CPC. The setting time was determined using a Vicat apparatus bearing a 300-g needle of 1 mm in diameter, and the initial setting time was measured according to a previously reported procedure [15]. The setting time data have been reported as the time taken from the start of mixing to the time when the needle failed to pierce the test specimen to a point 10 mm from the bottom of the mold. These tests were performed at temperatures of 16, 18, 20, 22, and 25 °C. The room temperature used in the current study was set to the same level as a general operating room, as defined by the *Guideline for prevention of surgical site infection* [16]. The average value of at least three tests was calculated for each specimen.

2.2.3 SEM, XRD, and Fourier-transform infrared spectra of CPCs and P-CP

The morphology of three hardened CPCs (CABC, CAC, and Com-CPC) and P-CP were examined by SEM. Hardened bodies were constructed from the three CPCs according to the method described below. The powder components were mixed with the liquid components for 1 min, and the resulting slurries were poured into cylindrical molds (6 mm in diameter and 15 mm in height), which were held for 100 h at 37 °C in a 50 % humidified atmosphere. The resulting hardened bodies were lyophilized and then they were polished with a No. 1000 sand paper for 5 min, then washed with distilled water in an ultrasonic cleaner for 1 min each, and finally dried at 25 °C for 1 day. Their cross-surfaces were examined by SEM.

For the analysis of their crystal phases, the hardened bodies were pulverized with a mortar, and the XRD patterns of the resulting powdered novel CPCs were examined

Table 2 Composition of calcium sodium phosphate (CSP)

	Chemical composition in feed: g (wt%)				Phase composition in crystal	
	Dibasic calcium hydrogen phosphate dihydrate	Calcium carbonate	Disodium phosphate dodecahydrate	Distilled water	$CaNaPO_4$	$Ca_6Na_3(PO_4)_5$
CSP	54.4 (2.36)	109 (4.72)	145 (6.28)	2,000 (86.64)	0.62	0.38

CSP calcium sodium phosphate

using XRD apparatus. The Fourier-transform infrared (FT-IR) spectra of the novel CPCs were also measured using a Spectrum One FT-IR spectrometer (Perkin Elmer Japan Co., Ltd., Kanagawa, Japan).

2.2.4 *Compressive strength of CPCs*

The compressive strengths of CABC, CAC, and Com-CPC were measured. The three CPCs were hardened separately in a split cylindrical mold (6 mm in diameter and 15 mm in height) at room temperature for 15 min and then removed from the mold. Following a 5-day period of hardening in air, the compressive strength properties of the materials were measured.

To examine the compressive strengths of these materials under conditions effectively simulating those of the living environment, the test specimens (CABC, CAC, and Com-CPC) were prepared as follows. One minute after initiating the mixing process, each cement paste was placed in a split cylindrical mold (6 mm in diameter and 15 mm in height) at room temperature. Following 5 min in the molds, the cements were placed in 10 ml of physiologic saline (0.9 wt% NaCl solution, Terumo Corp., Tokyo, Japan) per one sample at 37 °C and mixed for 15 min before being removed from the molds and placed in fresh physiologic saline for periods of 0.5, 2, and 24 h.

The compressive strengths of the samples were subsequently measured using a universal testing machine (AGA-500A Autograph; Shimadzu Co., Ltd., Kyoto, Japan) at a crosshead speed of 1 mm/min. The average value of at least three tests was calculated for each specimen.

2.2.5 *Examination of apatite-forming ability of the CPCs and P-CP in SBF*

The apatite-forming abilities of the four materials were measured in a simulated body fluid (SBF). Cylindrical samples (6 mm in diameter and 15 mm in height) of CABC, CAC, and Com-CPC, also P-CP were soaked in 15 mL of a SBF with ion concentrations almost equal to those of human blood plasma (i.e., $Na^+ = 142.0$, $K^+ = 5.0$, $Mg^{2+} = 1.5$, $Ca^{2+} = 2.5$, $Cl^- = 147.8$, $HCO_3^- = 4.2$, $HPO_4^{2-} = 1.0$, and $SO_4^{2-} = 0.5$ mM) [17] at 37 °C for 1, 3, and 7 days. The SBF was replaced every 24 h. After 1, 3, and 7 days, the samples were gently washed twice with distilled water, and examined by SEM (SU1510; Hitachi, Tokyo, Japan) to measure the formation of apatite on their surfaces.

2.3 Animal experiments

2.3.1 *Surgical procedure*

The four materials were implanted in the femoral condyle of 64 healthy, skeletally mature, male Japanese white rabbits that weighed between 2.8 and 3.2 kg. The protocol was approved by the Animal Ethical Committee of Kyoto University and performed in accordance with the National Guidelines for the Care and Use of Laboratory Animals.

The rabbits were anesthetized with an intravenous injection of sodium pentobarbital (0.5 mL/kg), and the local administration of a 0.5 % lidocaine solution. The animals were immobilized on their back and their hind limbs were shaved and disinfected with povidone-iodine. A 1.5-cm longitudinal skin incision was made on the medial side of the knee and the fascia and periosteum were incised and retracted to expose the femoral condyle.

Following the exposure of the distal femoral condyle, a 1.0-mm pilot hole was drilled. The hole was gradually widened with hand drills of increasing size until a final defect of 6 mm in width was created from the medial to the lateral condyle. After irrigating the hole with physiologic saline, test specimens were implanted in the hole, perforating the femoral condyle and protruding from the medial

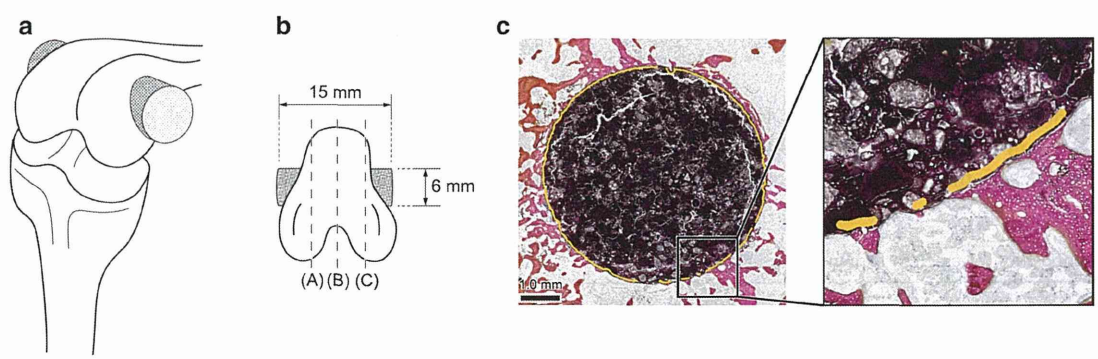

Fig. 1 Schematic drawing of the implanted site at a rabbit's femoral condyle and histomorphometric analysis measured on histological slides. **a** Implanted site at a rabbit's femoral condyle. **b** Three sections of each sample for histomorphometrical analyses: (*A*) medial condyle, (*B*) intercondylar fossa, and (*C*) lateral condyle sections. **c** Bone-material contact index = the fraction of bone contact at the outer perimeter of the implant (*yellow line*)/circumference of the material (Color figure online)

to the lateral cortex (Fig. 1a). This surgery was performed in both of the rabbit's hind legs, with one defect being created in each condyle. Test specimens were made from the four different materials, including (1) CABC, (2) CAC, (3) Com-CPC, and (4) P-CP. The test specimens, which were 6 mm in diameter and 15 mm in height, were implanted into the condylar defects in a randomized manner ($n = 8$), and the fascia and skin were closed layer by layer using nylon sutures. The animals were then housed individually in standard rabbit cages, where they were fed standard rabbit food and allowed free access to water.

After 4, 12, 26, and 52 weeks of implantation, the rabbits were euthanized using an overdose of intravenous sodium pentobarbital, and the femoral condyles were harvested for evaluation.

2.3.2 Histological examinations

Eight samples from each group for each time point following on from the initial implantation were fixed in 10 % phosphate-buffered formalin for 14 days and then dehydrated in serial concentrations of ethanol (i.e., 70, 80, 90, 99, and 100 vol. %), with 3 days at each concentration.

The samples were then embedded in polyester resin and cut into sections of 1,000 μm in thickness using a peak saw (BS-3000CP; Exact-Apparatebau, Norderstedt, Germany) positioned perpendicular to the axis of the sample. These sections were subsequently polished to a thickness of 30–50 μm using a grinding-sliding machine (Microgrinding MG-4000; Exact-Apparatebau). One section from each sample was examined SEM, whereas the others were stained with Stevenel's blue and Van Gieson's picrofuchsin. The resulting histological slides were subjected to a thorough microscopic analysis using a digital microscope (DSX 500; Olympus, Tokyo, Japan).

2.3.3 Histomorphometrical analyses

To evaluate osteoconductivity and bioresorbability properties of the materials, the bone-material contact indices and material absorbed ratios of the materials were measured on the histological slides stained with Stevenel's blue and Van Gieson's picrofuchsin using a transmitted light microscope (model Eclipse 80i; Nikon, Tokyo, Japan) equipped with a digital camera (model DS-5M-L1; Nikon). These parameters were then calculated on a personal computer using Adobe Photoshop 7.0 (Adobe System Inc., San Jose, CA, USA) and Image J 1.45 (National Institute of Health, Bethesda, MA, USA). Three sections of each sample were analyzed, including the medial condyle, intercondylar fossa, and lateral condyle sections (Fig. 1b). Eight samples were analyzed for each type of implant for each time point following on from the initial implantation.

The bone-material contact index was calculated for each type of CPC as follows:

Bone-material contact index = the fraction of bone contact at the outer perimeter of the implant/circumference of the material (Fig. 1c).

The material absorbed ratio was evaluated for each type of CPC, and calculated as follows:

Material absorbed ratio (%) = {1 − (Areas of remaining material)/(Area of a circle 6 mm in diameter)} × 100.

2.4 Statistical analysis

All of the data were recorded as the mean ± standard deviation (SD). The compressive strengths of the materials were assessed using the Wilcoxon signed-rank test, whereas the other measurements were assessed using one way analysis of variance followed by Tukey–Kramer multiple comparison post hoc tests at each time point. The JMP 9 software (SAS Institute, Cary, NC, USA) was used for the statistical analyses. Differences of $p < 0.05$ were considered statistically significant.

3 Results

3.1 Results and material characterization

3.1.1 SEM and XRD of the CSP powder

The powdered CSP particles were round and smooth in appearance with an average diameter of 130 μm. SEM micrographs of this material are shown in Fig. 2a.

Figure 2b shows an XRD pattern of the powdered CSP. The crystals were refined and contained 62 % $CaNaPO_4$ and 38 % $Ca_6Na_3(PO_4)_5$ (Table 2).

3.1.2 Setting time at various room temperatures

Figure 3 shows the setting times of the CPCs at different temperatures. The setting times of CABC were 10.2 ± 0.3, 8.5 ± 0.0, 6.7 ± 0.3, 5.7 ± 0.3, and 3.0 ± 0.5 min at 16, 18, 20, 22, and 25 °C, respectively, whereas those of CAC were 22.2 ± 0.8, 19.2 ± 0.3, 16.3 ± 0.3, 11.3 ± 0.6, and 9.7 ± 0.3 min at 16, 18, 20, 22, and 25 °C, respectively. The corresponding values for Com-CPC were 105.5 ± 0.5, 45.2 ± 1.0, 40.3 ± 1.5, 21.8 ± 0.6, and 12.3 ± 0.8 min, respectively. In general, the setting time decreased as the temperature increased. This result suggested that the reactions of the CPCs were temperature-dependent. The setting times of CABC were statistically significantly shorter than those of CAC and Com-CPC at each of the temperatures tested (for p values, please see the figure caption), and the setting times of CAC were statistically significantly shorter

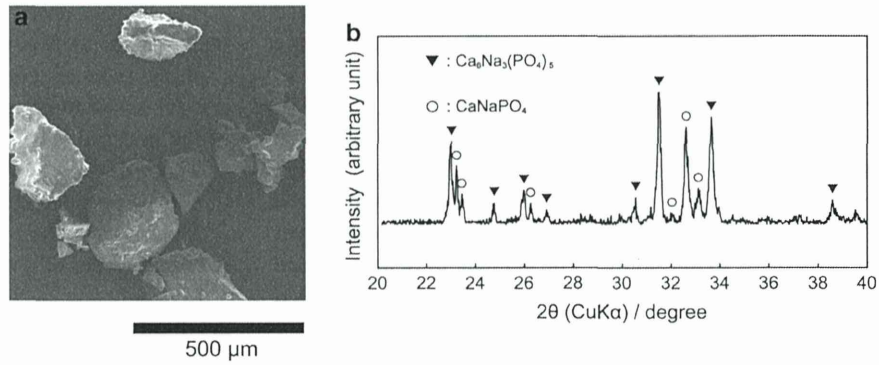

Fig. 2 SEM and XRD of the CSP powder. **a** An SEM micrograph of powdered CSP. **b** XRD pattern of powdered CSP. *closed inverted triangle* represents $Ca_6Na_3(PO_4)_5$ and *open circle* represents $CaNaPO_4$

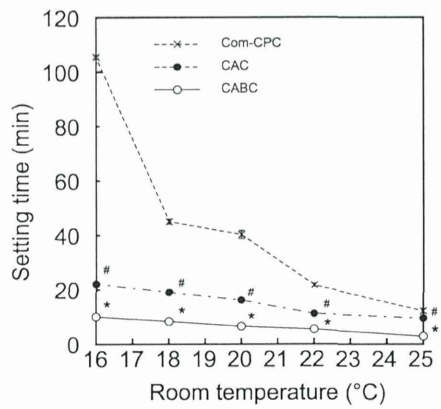

Fig. 3 Setting times of the three CPCs at different temperatures. The p values of CABC vs Com-CPC, CABC vs CAC, and CAC vs Com-CPC were 1.0×10^{-10}, 4.7×10^{-7} and 1.0×10^{-10} at 16 °C, 1.3×10^{-9}, 1.9×10^{-6} and 9.5×10^{-9} at 18 °C, 2.0×10^{-8}, 3.2×10^{-5} and 1.5×10^{-7} at 20 °C, 4.3×10^{-8}, 2.2×10^{-5} and 5.7×10^{-7} at 22 °C, and 2.1×10^{-6}, 1.5×10^{-5} and 2.5×10^{-3} at 25 °C, respectively. *$p < 0.0001$ vs CAC and Com-CPC, #$p < 0.01$ vs Com-CPC

than those of Com-CPC at each of the temperatures tested (for p values, please see the figure caption).

3.1.3 SEM, XRD, and FT-IR spectra of CPCs and P-CP

Figure 4 shows SEM micrographs of the three CPCs after they had all completely hardened and an SEM micrograph of P-CP: (a) CABC, (b) CAC, (c) Com-CPC, and (d) P-CP.

Figure 5a shows the XRD patterns of the novel CPCs. The XRD patterns of CABC and CAC contained only small XRD peaks corresponding to α-TCP and CSP. Figure 5b shows the FT-IR spectra of CABC and CAC. The FT-IR spectra of α-TCP and CSP did not contain an absorbance peak corresponding to the carboxylate ion ($-COO^-$: 1,610–1,550 cm^{-1}). In contrast, the FT-IR spectrum of CABC and CAC contained an absorbance peak corresponding to the carboxylate ion but did not contain a peak for citric acid (C = O: 1,750–1,706 cm^{-1}).

3.1.4 Compressive strength of CPCs

Figure 6a shows the maximum compressive strengths of the CPCs after they had been held for 5 days. The maximum compressive strengths were 86.0 ± 9.7, 73.4 ± 4.2, and 73.1 ± 9.0 MPa for CABC, CAC, and Com-CPC, respectively. No statistically significant differences were observed in the maximum compressive strengths of CABC, CAC, and Com-CPC.

Figure 6b shows the compressive strengths of the CPCs with physiologic saline. The compressive strengths of CABC were 21.6 ± 1.2, 26.7 ± 3.7, and 40.4 ± 2.8 MPa after 0.5, 2, and 24 h, respectively. The compressive strengths of CAC were 12.6 ± 2.6, 11.2 ± 0.9, and 23.4 ± 5.0 MPa after 0.5, 2, and 24 h, respectively. The corresponding values for Com-CPC were 9.8 ± 0.4, 10.7 ± 1.4, and 33.6 ± 8.8 MPa, respectively. CABC showed a compressive strength that was statistically significantly higher than Com-CPC at 0.5 and 2 h ($p = 0.040$ and 0.022, respectively). CABC showed statistically significantly higher compressive strength than CAC at 0.5, 2 and 24 h ($p = 0.040$, 0.022 and 0.038, respectively).

3.1.5 Apatite-forming ability of CPCs and P-CP in SBF

Apatite was observed on the CABC and CAC surfaces after 1 day in SBF but not on the Com-CPC and P-CP surfaces. Apatite was first observed on the Com-CPC surface after 7 days in SBF, but not on that of the P-CP surface. The SEM images of the test samples after 3 days in SBF are shown in Fig. 7. At this time point, the apatites on the CABC and CAC surfaces had increased in size (white arrows), whereas no apatite could be observed on the Com-CPC and P-CP surfaces.

3.2 Results of animal experiments

All 64 rabbits exhibited good health and did not show any wound complications. At the end of the implantation periods, a total of 128 surrounding tissues were harvested

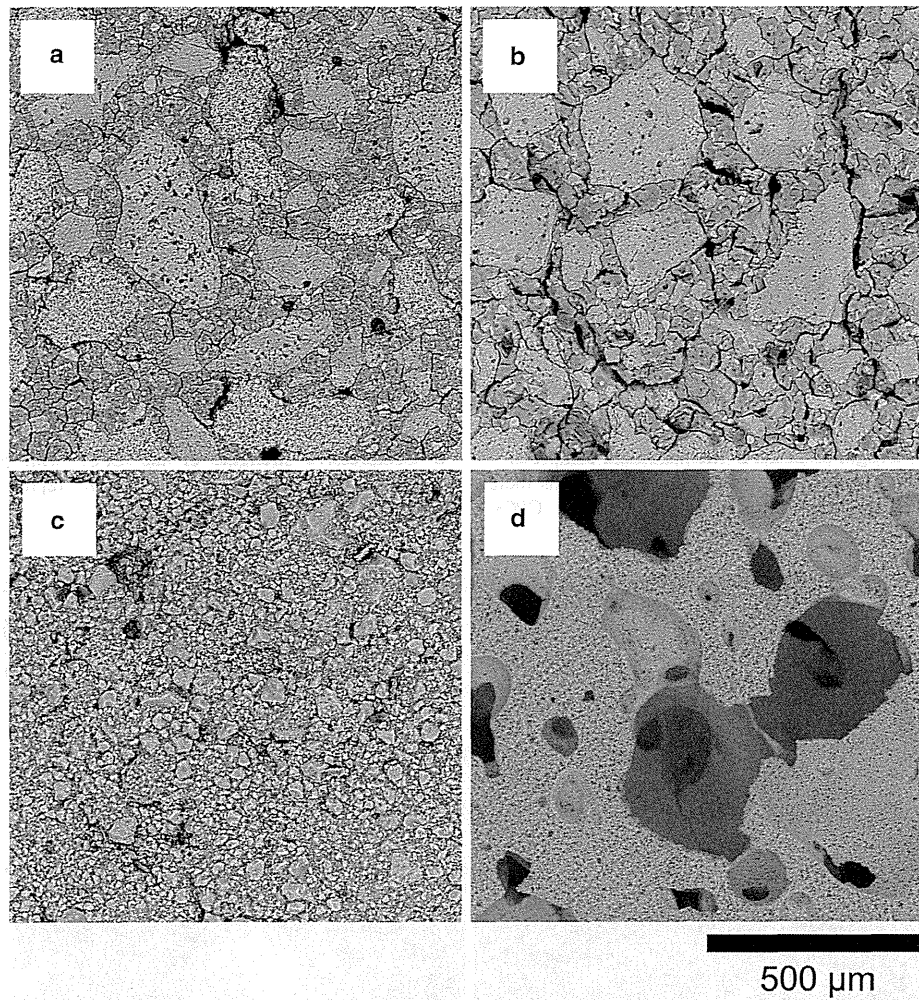

Fig. 4 SEM micrographs of the three CPCs after they had completely hardened and P-CP; **a** CABC, **b** CAC, **c** Com-CPC, and **d** P-CP

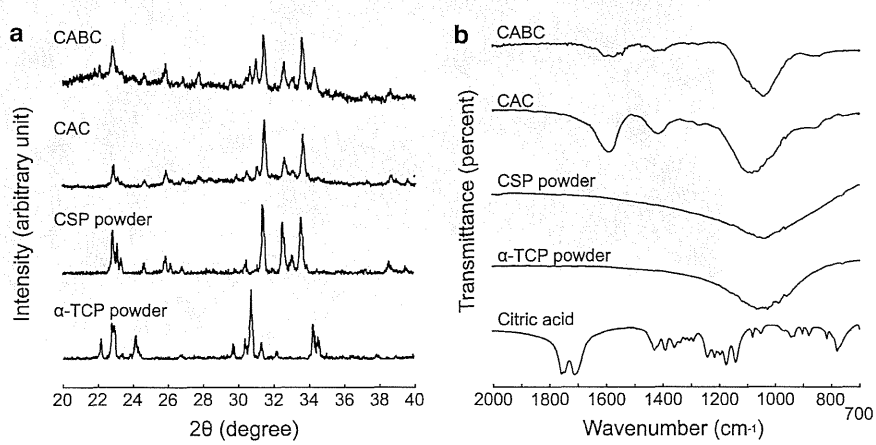

Fig. 5 XRD, and FT-IR spectra of CABC and CAC. **a** XRD patterns of CABC and CAC, **b** FT-IR spectra of CABC and CAC